SINERGI Vol. 30, No. 3, October 2026: 851-862
http://publikasi.mercubuana.ac.id/index.php/sinergi
http://doi.org/10.22441/sinergi.2026.3.013

Microstructural and mechanical enhancement of resistance spot welding with initial gap using TiO_2 and Fe nanoparticle interlayers

Bilal Mohammed Qasim*, Ahmed Yashar
Department of Mechanical Engineering, Faculty of Engineering, Kirkuk University, Iraq

Abstract
The welding time, current intensity, and electrode pressure are critical parameters in resistance spot welding. The initial gap often arises during spot welding of automotive repair structures, hindering the attainment of excellent welds. These variables evidently affect welding quality, hence compromising the structural integrity and safety of the vehicle. This study's novelty lies in the use of two interlayer types in a spot-welding technique to produce microstructurally strong lap joints. It assesses the influence of interlayer composition on microstructural evolution and the formation of the weld nugget under tensile shear stress. The influence of three initial gap dimensions (0.5 mm, 1 mm, and 1.5 mm) was analyzed using two varieties of interlayer nanoparticles (iron particles and TiO_2) to fill the gaps by compaction, excluding the incorporation of filler material; the investigation evaluated the mechanical properties of the welded joints. The results demonstrated a significant increase in joint strength relative to a direct connection without an interlayer; this enhancement is influenced by the gap size and the type of nanoparticles used to fill it. At a plate gap of 0.5 mm, both iron and TiO_2 particles significantly enhance weld strength; this effect is also observable at a separation of 1 mm. Nonetheless, when the gap widened to 1.5 mm, adding an interlayer did not affect the strength of the welded plates. Results demonstrate that nanoparticle interlayers substantially affect gap size by enhancing welding conditions in vehicle repair. The study clarifies the importance of nanoparticle augmentation in closing gaps, hence enhancing joint efficacy and structural integrity.

This is an open-access article under the CC BY-SA license.

Keywords:
Initial Gap;
Mechanical Properties;
Microhardness;
Nanostructured Interlayer;
Spot Welding;

Article History:
Received; September 14, 2025
Revised: March 5, 2026
Accepted: April 20, 2026
Published: October 2, 2026

Corresponding Author:
Bilal Mohammed Qasim
Mechanical Engineering Department, Kirkuk University, Iraq
Email:
bilal196932@uokirkuk.edu.iq

INTRODUCTION

Resistance Spot Welding (RSW) is a technique for fusing two or three metal sheets at specific points along their interface. Spot welding for permanent assembly is frequently employed in manufacturing industries because of its benefits, including repeatability, low labor costs, high production rates, and minimal equipment requirements. RSW is widely used to weld thin sheets of ferrous and nonferrous metals, including mild steel, copper, and aluminum. Sheet metal welding is used in the automotive body, household goods, and aircraft industries. Three thousand to six thousand resistance spot welding techniques account for 90% of the total welding workload in modern automobile body structure assemblies. The initial gap adversely affects welding quality and weld strength by reducing the peak load and production speed in high-volume manufacturing, resulting in a 12% increase in structural rework rates [1]. This technique is also employed for the repair of economic equipment [2][3]. Features such as current magnitude, welding duration, applied force, and holding time all affect the effectiveness of spot welding.

The environment significantly impacts the formation of nugget diameter and tensile strength [4, 5]. During standard vehicle operation and in the event of a collision, RSW reliably withstands a range of external forces. Consequently, misalignment occurs due to the gap between the welded plates and adversely affects the overall quality of the welding process in vehicle body production [6][7]. Furthermore, stamping variations in thin plate structural components, process clamping inaccuracies, and other discrepancies during the body assembly process result in an overall deviation in body manufacture, leading to the emergence of an initial gap between the thin plates [8].

Address the gap in the shear behavior of localized Heat Affected Zones (HAZs) and enhance the comprehension of their mechanical behavior under diverse stress conditions. It will enhance precise fracture prediction by stress triaxiality-based fracture criteria. The observation revealed that distortion surrounding the corona-bond varied according to the gap. Also, the gap reduced the joint strength despite the nugget being sufficiently sized. These results suggested that regulating the gap is crucial for maintaining the quality of RSW [9]. Although fabrication quality is excellent, the majority of sheet welds do not achieve a zero gap between sheets; occasionally, a geometric variation gap appears. One important factor that contributes to considerable deformation during maintenance is the space between the welded sheets [7][10].

The most effective test for welded sheets is the tensile shear test, which indicates mechanical properties. Test failures can be categorized into two groups. Initially, Pullout Failure (PF) occurs from the Base Metal (BM) and may also commence from the Heat Affected Zone (HAZ) or the HAZ-Fusion Zone (FZ) junction, while the fusion zone endures the load without failure. The second type of failure is Interfacial Failure (IF), which initiates at the notch and advances until it reaches the Fusion Zone (FZ). This failure results in the separation of the welded sheets under the tensile test force. A large reduction in the welding current indicates a decrease in joint strength. In terms of energy absorption, the PF outperforms other types and withstands more applied test forces before failure [11,12].

The functional features and superior structure of materials such as carbon nanotubes and graphene present considerable potential, providing these nanoparticles with extensive applications across various industrial sectors [13]. Incorporating nanoparticles between welded sheets reduces existing gaps and enhances both interference and heat transmission [14]. This enhancement helps reduce microscopic defects that may occur during the welding process.

The benefit of using nanoparticles is evident in the enhancement of weld quality, as shown in several studies, mostly conducted by researchers concentrating on zero or near-zero gaps, who assessed the bonding strength of nanoparticles in such situations. The use of interlayers such as carbon nanoparticles or graphite enhances thermal conductivity in the weld zone and improves mechanical strength and microstructure; however, these improvements have not been well explored. Nonetheless, a substantial research gap persists concerning the impact of these interlayer materials on the strength of welded plates with an initial gap.

Adding nanoparticles can improve mechanical properties such as bond strength, stiffness, weld durability, and toughness, while still maintaining thermal and mechanical characteristics [15][16]. Mechanical qualities are also enhanced when titanium dioxide nanoparticles occupy the gaps in welded sheets. Enhancing characteristics can be achieved by including various forms of titanium dioxide, such as TiO_2, TiO, and Ti_2O_3, which increase the nucleation rate and delay the formation of ferrite grains. The successful augmentation of nucleation sites for intragranular acicular ferrite in welding zones using welding procedures [17].

The interlayer nanoparticles encompass a range of materials beyond titanium dioxide to enhance weld bond strength. Other interlayers, including copper, iron, cerium, titanium, nickel, and zinc-based alloys, have been utilized, resulting in improvements for both similar and dissimilar welded sheets [18,19,20]. Graphene interlayers are used to improve the mechanical properties of welded AISI-1008 steel sheets with an initial gap [21].

These findings bridge the knowledge gap regarding the shear behavior of localized HAZs and enhance our understanding of their mechanical behavior under varying stress conditions. It will assist in accurate fracture prediction using stress-triaxiality-based fracture criteria [22].

Previous studies have explored the experimental and theoretical effects of the initial gap on weld strength performance in spot welding. This study aims to evaluate the ratio of iron and TiO_2 nanoparticles as an intermediate layer with a predefined initial gap and to correlate the mechanical performance with the microstructure; this is where the novelty of the research lies. The methods used to determine the results facilitate understanding of the relationship between the gap geometry and interlayer composition. This subject has not been explored in other studies of AISI 1008 steel.

This study examines considerable discrepancies in the understanding of the impact of various initial gaps on resistance spot welding under mechanical loads, as shown in Figure 1, and in the microstructural analysis.

EXPERIMENTAL DETAILS

Material and Method

AISI 1008 carbon steel plates were chosen as the foundational materials and are utilized extensively in several industries, including automotive chassis and the production of household appliance frames. It is among the most prevalent varieties of carbon steel. A 1-mm sheet thickness was used as the base metal for RSW. All samples were mechanically polished, and impurities were removed with acetone after cleaning before the welding process began.

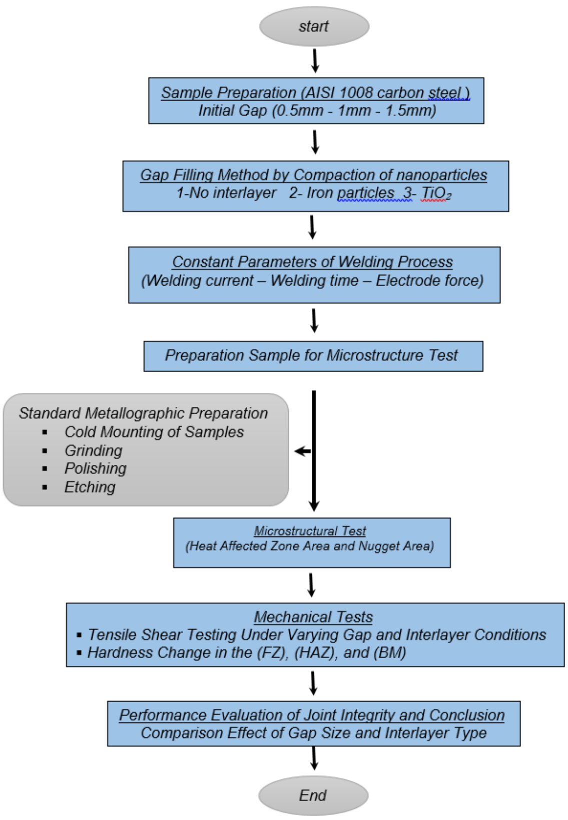

Figure 1. The flowchart showing the main stages of the investigation

The chemical composition of the main material, as determined using a standard quantitative meter, is provided in Table 1. The mechanical properties of the main material were assessed in accordance with ASTM E8M, using a standard tensile test [23]. Table 2 presents the mechanical properties of the examined plate [24].

AISI 1008 carbon steel plates with 145 mm in length, 135.0 mm in width, and 1.0 mm in thickness were selected as the basic materials, with the weld point positioned at the center of the overlap.

The required RSW specimens with Initial Gap Between Plates (IGBP) are produced using weld gap blocks of three distinct thicknesses (0.5 mm, 1.0 mm, and 1.5 mm). These gap blocks possess high hardness to ensure welding quality by preventing deformation under pressure.

The weld gap blocks are positioned centrally between the welded plates, as seen in Figure 2. Upon completion of the welding, the gap blocks may be extracted from both sides. The welding gap is sealed with a Kapton tape insulator, which ensures that the current flows in the nugget zone; this tape maintains stability across a broad temperature range of 269℃ to 400℃. To maintain the symmetry of the weld structure and prevent uneven deformation of the top and bottom sheets caused by positional deviation, a curved-jaw locking clamp plier apparatus is necessary for welding experiments.

An experimental setup was used to demonstrate the properties of spot welding. In the welding method, the electric current flows through the plate and the contact area with the electrode, and the resulting resistance heating melts the joining surface, thereby achieving the connection. The electrode force was set to a constant 6.9 kN, with a welding current of 7 kA and a total welding time of 4 seconds in constant-maintained current mode.

Table 1. Chemical Composition of AISI-1008 Steel Utilized as Base Metal

Item	C	Mn	Si	S	P	Fe
Prec. (%)	0.065	0.204	0.095	0.017	0.018	Base

Table 2. Mechanical Properties of AISI-1008 Steel Employed as Base Metal

Yield Strength MPa	Tensile Strength MPa	Elongation %
185	330	43

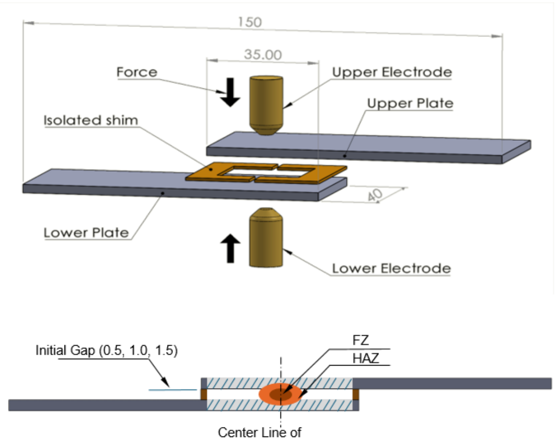

Figure 2. Welded plate with initial gap (a) from the top, (b) from an isometric perspective, and (c) from the front part of the nugget region.

The values for current, total welding time, and electrode force were found by doing several experimental tests to get the highest shear force before the welding C15000 failed.

Three samples were generated for each set of investigated factors, and the process signals from each welding site were gathered and recorded for further study. Four distinct welding gaps are used for applications without particles. Initially, a zero gap was established between the welded plates, followed by introducing initial gaps of 0.5 mm, 1.0 mm, and 1.5 mm prior to welding. These four distinct gaps were also used for both iron and TiO_2 particle interlayers. The nanoparticles were introduced into the gap by applying equal quantities and dispersing them across the welding zone.

Copper-zirconium alloy is used as electrode material in the experimental welding. To reduce wear at the electrode tip and maintain consistency in the welding process, the electrode diameter was kept at 5 mm by polishing the tip after welding 10 sheets. Cooling was used throughout the welding process to ensure repeatability and to prevent changes in welding conditions.

Microstructure Test

The lap-welded region of the original specimen was longitudinally sectioned at the center of the weld, resulting in three categories of welded specimens: welded plates without an interlayer, welded plates using iron as an internal particle, and welded plates utilizing TiO_2 as an interlayer. The three distinct interlayers were bisected at the weld zone and subsequently subjected to standard metallographic preparation, including cold mounting, grinding the sample faces, polishing, and final etching with 2% Nital. An optical microscope and field-emission electron microscopy were employed to examine the microstructure at various locations in the resistance spot welds.

Hardness and Tensile-Shear Test

The hardness test of the spot welds was conducted using Vickers microhardness at a 45° angle to the transverse direction of the weld nugget. The test starts by cleaning and polishing the specimen surface. Using an INNOVATEST Inspection Equipment machine with a maximum load of 30 grf, following the methods specified in ASTM E384.

The tensile-shear test was conducted to assess the mechanical performance and failure mode of the tested samples. Figure 1 illustrates the dimensions of the tensile-shear sample. Tensile-shear tests were conducted at a crosshead speed of 10 mm/min using 10-ton UNIVERSAL testing equipment.

RESULTS AND DISCUSSION

Microstructure Observation Results

Figure 3 (a) displays optical microscope images of the microstructure of various welded samples in the transverse cross-section. All the shapes of nuggets appear as elliptical, resulting in the appearance of three primary zones: BM, HAZ, and FZ. The regions exhibit variations in grain morphology and microstructure attributable to the distinct thermal cycles (cooling rates to reach ambient temperature and peak temperatures) experienced by each region. The plates produced by the deep drawing process exhibit a ferrite structure with a stretched microstructure, which remains consistent even after spot welding [12]. The heat generated during spot welding causes rapid melting and solidification of the metal, leading to changes in the structure and morphology between the heat-affected zone and the base material grains. The rapid melting and solidification processes in spot welding led to a microstructure that is distinctly characterized by a martensitic structure in the fusion zone [24]. Coarse lath martensite is located at the core of the welding nugget and extends outward along the central axis. The martensite crystals decrease in size from the nugget to the HAZ, creating a transformation region between the HAZ and the BM. The martensite and ferrite grains are included in the metallographic structure [6][15].

Figure 3 (b) shows the nugget added in the absent interlayer and the gap equal to zero. A confluence line separates the two welded sheets, and lath martensite grains are found around the line. Figures 3 (c) and (d) depict the confluence line and outside the nugget zone, respectively, for a gap equal to 1.0 mm, with the addition of iron particles as an interlayer. The lath martensite grains are found around the line, while surpassing iron particles that exit the nugget zone and solidify between plates.

The addition of TiO_2 nanoparticles with an initial gap equal to 1.0 mm microstructure is revealed in an accumulated phase at locations between the yellow dashed line. This is shown in Figure 3 (e). TiO_2 nanoparticles can be observed in the weld nugget zones with lath martensite; these particles can act as barriers between the weld plates, influencing the heat transfer rate and grain size. This procedure helps improve the joint's load-bearing capacity.

A defect associated with spot welding is the pit defect, which manifests at the center of the nugget, as illustrated in Figure 3 (f). This defect occurs during the refinement of grains in the melted steel plate of the welded zone, as the welding crystallizes upon cooling. It arises during the rapid cooling and solidification shrinkage phase.

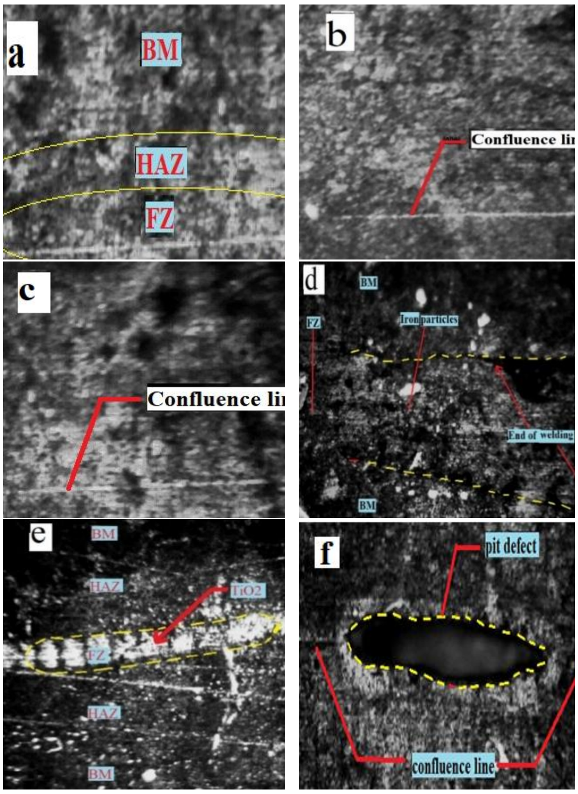

Figure 3. Weld nugget cross-section illustrating (a) micromorphology of the (FZ), (HAZ), and (BM), (b) nugget zone exhibiting zero gap without interlayer addition, (c) nugget zone with the inclusion of iron particles as an interlayer at a 1 mm gap, (d) additional iron particles discernible between the welded plates, (e) nugget zone incorporating TiO_2 nanoparticles, and (f) spot welding exhibiting pit defects

Relationship between nugget profile and heat-affected zone area

Figure 4 (a) shows the morphologies of the cross section of the weld regions in both the longitudinal and transverse directions with three distinct interlayer particles for a 1.0 mm starting gap. The black elliptical line shows the nugget, while the red elliptical line represents the HAZ. In the absence of interlayer particles, as depicted in Figure 4(b), the nugget's diameter is minimal compared to the other two interlayer particle conditions, and voids are present between the two welded plates. The diameter of the nugget is about the same in length for both iron in Figure 4 (c) and TiO_2 particles in Figure 4 (d). This indicates that the horizontal cross-sectional shape of the nugget enlarges, enabling it to withstand greater tensile loads before failure, and that voids are observed in iron particles.

Nugget formation

The various metals joined by spot welding exhibit distinct characteristics within the weld zone. The incorporation of two particles (iron and TiO_2) is anticipated to alter the nature of intermetallic composites in the nugget region during welding, hence affecting the nugget area and heat-affected zone, which subsequently influences joint strength [7].

A comparison of the nugget area between interlayer iron particles and TiO_2 Nanoparticles, with error bars, as well as the area without any additions, is illustrated in Figure 5. Measurements linked to the nugget area and HAZ study were performed using FIJI software.

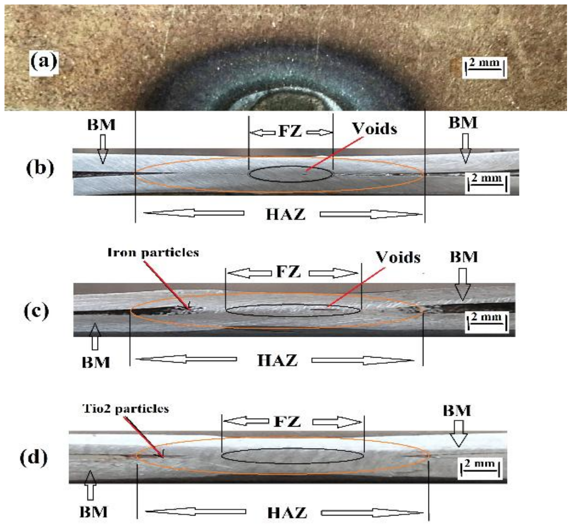

Figure 4. Cross-sectional profiles of a 1.0 mm gap: (a) top view of half nugget, (b) without particles, (c) with iron particles interlayer, (d) with TiO_2 particles interlayer

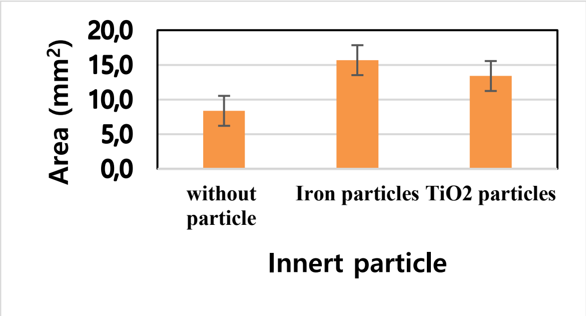

Figure 5. Nugget area of two types of interlayer particles and none for a 0.5 mm gap

The findings indicate that incorporating interlayer iron particles and TiO_2 Nanoparticles into a 0.5 mm gap enhances mechanical properties and yields the largest fusion zone, 15.673 mm², when iron particles are added. In contrast, the fusion zone measures 13.390 mm² when only TiO_2 nanoparticles are introduced. This progression demonstrates that nugget growth is influenced by heat distribution and the localization of melting.

The increased heat at the melting point directly affected the HAZ, which expanded with the addition of TiO_2 and iron nanoparticles, as shown by the error bars in Figure 6. The HAZ area increased from 137.858 mm² without particles to 165.882 mm² (20.3% increase) with TiO_2 nanoparticles and 183.433 mm² (33% increase) with iron particles. This indicates greater thermal diffusion in the HAZ, leading to changes in grain size and structural toughness that affect the mechanical properties of the welded plates.

Data on nugget area and standard deviation (0, 0.5 mm, 1.0 mm, and 1.5 mm gaps) illustrated in Figure 6 indicate that the incorporation of iron and TiO_2 particles significantly improves the nugget area in spot welding across various gap sizes compared to the absence of interlayer particles.

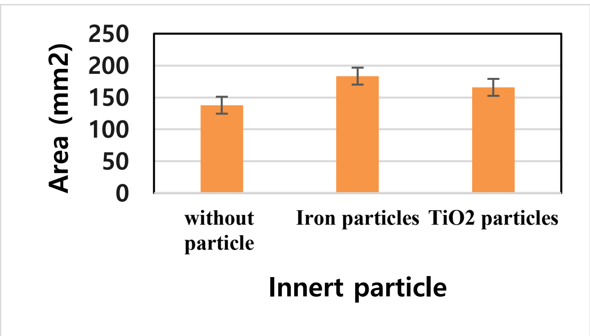

Figure 6. Heat-affected zone area of two types of interlayer particles and none for a 0.5 mm gap

The influence of nanoparticles in the contact region between welded sheets with a gap enhances the weld area, resulting in the production of a martensitic structure. This phenomenon may be attributed to the augmented Joule heating theory, caused by the increased electrical resistance at the contact, attributed to the particles situated between the layers. The iron interlayer particles exhibit elevated thermal conductivity and impede heat dissipation, whilst the TiO_2 nanoparticles act as thermal barriers, modulating heat transfer.

This enhancement in stability and fusion efficiency is particularly evident at intermediate gap sizes. The data unequivocally indicate that incorporating interlayer particles (iron and TiO_2) markedly enhances the nugget area in spot welding across all gap sizes relative to samples devoid of particles and that it surpasses the traditional process in preserving nugget integrity.

To get the error bars shown in Figures 5, 6, 7 and 8, we averaged the three readings and then calculated their standard deviation. By dividing the standard deviation of the data by the square root of the number of measurements, the error is calculated, as shown in the graph.

Comparing nugget area and HAZ area results with and without the presence of interlayer particles, with iron and TiO_2 nanoparticles demonstrated in Figure 7 and Figure 8 respectively, reveals a significant enhancement in thermal effect and an increase in HAZ area, this improvement in thermal conductivity and energy absorption leads to an increase in the HAZ and standard deviation, for initial gaps (0, 0.5 mm, 1.0 mm and 1.5 mm). The increase in size is due to particles present between the layers. These particles allow heat to transfer more effectively between the plates in contact, thereby improving weld quality. A bigger HAZ then leads to improved ductility and stronger metallurgical bonding.

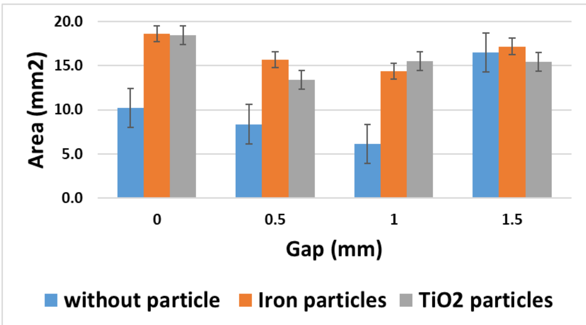

Figure 7. Nugget area dimensions for samples lacking iron and TiO_2 particles for tests at gap intervals of (0, 0.5 mm, 1.0 mm, and 1.5 mm)

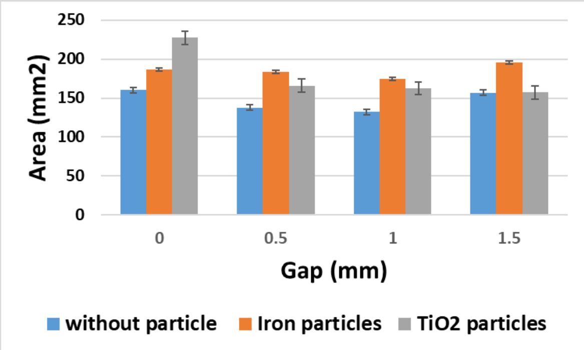

Figure 8. HAZ area dimensions for samples without iron and TiO_2 particles for gap measurements of (0, 0.5 mm, 1.0 mm, and 1.5 mm)

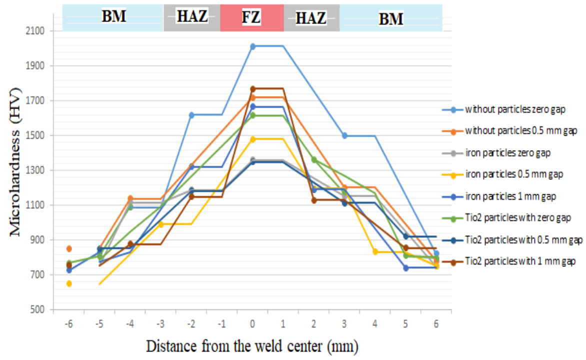

Figure 9. Microhardness graphs illustrating the hardness change in the (FZ), (HAZ), and (BM) with and without the incorporation of interlayer particles

Hardness Profile

Microhardness investigations of resistance spot-welded joints, incorporating interlayer iron particles and TiO_2 Nanoparticles, as seen in Figure 9, reveal a gradient from the BM to the HAZ and into the FZ. Rapid cooling in the FZ increases hardness, and the grains become refined in RSW [7]. The results without the interlayer show that the HAZ, BM, and the occurrence of coarser grains influence the hardness. When the gap is 0, maximum hardness is reached in BM, and when the gap is 0.5 mm, minimum hardness is reached. The interlayer with an iron-particle weld joint exhibits increased hardness in the interfacial zone due to the formation of brittle grain refinement when the gap is 1.0 mm. Hardness in the fusion zone decreases as the gap narrows, reaching its lowest value at zero gap. With TiO_2 or iron particles, the hardness shows a similar trend, with the maximum at a 1.0 mm gap and the minimum at zero gap. The increased hardness is attributed to grain refinement in the fusion zone due to the rapid cooling rate of resistance spot welding method.

There is a possibility that the heat-affected zone will exhibit a recrystallization region adjacent to the fusion zone and a region of partial recrystallization near the base metal. This can be ascribed to changes in temperature dependency [16]. All the original dislocations have been repaired within the recrystallization region, and the coarse grains have formed. On the other hand, larger grains persist in the region where recrystallization has occurred only in part. In this region, the initial dislocation has only been partially restored. The recrystallization of coarse grains and the existence of a zone that is devoid of dislocations are the causes of the softening region that forms in the heat-affected zone, which is in contrast to the fusion zone.

Tensile-Shear Test Results

For each distinct gap welding, three samples were examined. The results are illustrated in Figure 10, excluding nanoparticles between the plates. The findings of spot welding, when varying the gap between the two plates, reveal a nonlinear relationship between the mechanical performance of the welded plates and the magnitude of the gap. When plates are welded without a gap, the peak load reaches an average value of 5.4 kN, indicating robust bonding at the plate contact and optimal nugget formation [1]. The peak load magnitude and extension prior to rupture, with a 0.5 mm gap, changed the minimum average force and extension values before failure, reaching 4.2 kN. Extending the distance to 1.0 mm undermines the welding strength and elongation, as indicated by the nugget during inadequate fusion. Notably, at a distance of 1.5 mm, intermediate gaps exhibit optimal weld quality, achieving a maximum load of 5.8 kN before failure, indicating enhanced fusion in the nugget zone.

Results of a gap equal to zero are presented in Figure 11. The results are shown for both non-inert particles and the two interlayer iron and TiO nanoparticles. Robust joint integrity appears with the absence of inert particles, complete plate contact with zero gap, and continuous heat flow. The tensile shear test results show a peak load of 5.4 kN and an extension of 6.8 mm. When using iron particles, the peak load levels remain significantly elevated. TiO_2 particles served as a significant barrier within the weld zone, reducing the peak load to 4.9 kN and extending the weld by 3.5 mm when used as an interlayer.

The efficacy of spot welding is significantly affected by the 0.5 mm spacing and the use of inert particles, as illustrated in Figure 12.

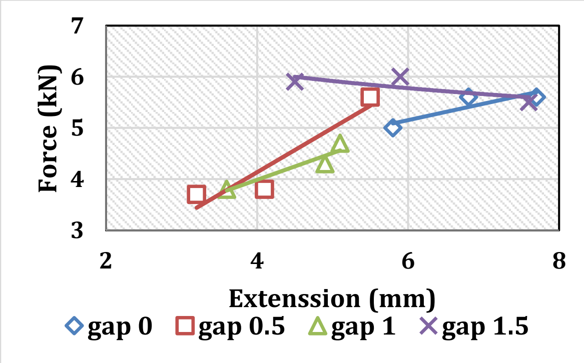

Figure 10. Peak load vs the extension of spot welding without inert particles and varying gaps

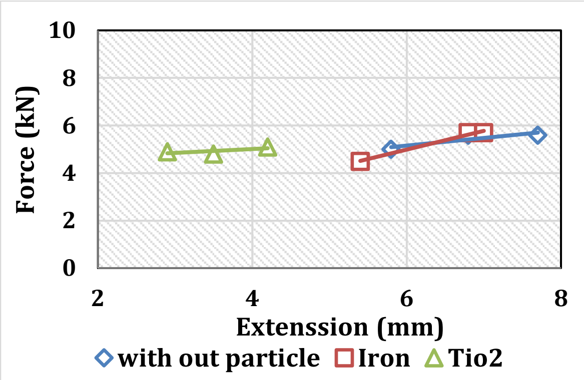

Figure 11. Peak load vs extension for inert particles in spot welding with zero gap

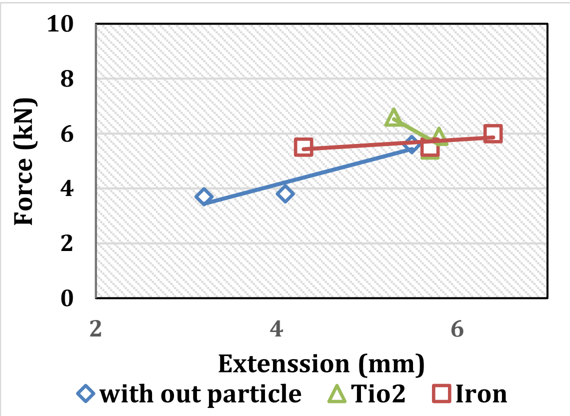

Figure 12. Peak load vs extension for inert particles in spot welding with 0.5 mm gap

In contact between plates without the addition of particles, the peak load exhibits a reduced average value of 5.0 kN with an extension of 3.1 mm. The minimal space between the plates restricts complete contact and heat transfer. The peak load increased with the incorporation of nanoparticles as an interlayer, primarily due to the enlargement of the weld nugget diameter; this increase in nugget area produced a restraining effect against shear failure [13], culminating in a peak load of 5.7 kN and an extension of 5.5 mm. The use of TiO_2 improved peak load and extension, achieving a peak load of 6 kN and an extension of 5.6 mm [20].

Effect of advantage the addition of inert particles between gaps equal to 1 mm is obvious, as shown in Figure 13. Without additional particles between the gaps, the minimum peak load reached 4.3 kN and 4.5 mm extension. The iron particles rising in the size of the nugget are due to the presence of particles between the layers.

These particles enhance heat transfer more effectively between the plates in contact; the peak load reaches 5.9 kN with a 6.3 mm extension. The incorporation of nanoparticles enhances thermal input in the welding area, leading to deeper and broader spot welds. The elevated heat conductivity of nanoparticles facilitates quick and uniform solidification in the nugget zone, hence diminishing thermal stress, deformation, and stress concentration [20]. The integration of TiO_2 exhibits notable shear-force resistance, with an average peak load of 5.0 kN and an elongation of 4.6 mm. The interaction of the molten nugget zone was augmented and disseminated when TiO_2 filled the vacuum.

As the space between welded plates expands to 1.5 mm, as seen in Figure 14. The efficacy of nanoparticle integration declines under insufficient pressure, leading to wider particle dispersion and poor maintenance of the current pathway. This resulted in a decrease in heat generated and transmission.

The performance of three distinct types of spot welds varies. The effect of adding nanoparticles decreases as the distance between the weld sheets increases, due to the reduced formation of an ideal nugget. Peak load results with and without inert particles: nearby in peak load, reaching 5.8 kN and a 6 mm extension without adding an interlayer. Incorporating iron particles into the interstice before welding diminishes joint strength and reduces the average peak load. This effect, influenced by heat transfer and metallurgical bonding, results in an average peak load of 4.7 kN and a 4.3 mm extension. The intermediate behavior of welded connections was achieved when TiO_2 was utilized as filler material in the gap. The average peak load attained was 5 kN, and the extension measured 4 mm.

Using one-way ANOVA with n=3, statistical analyses were conducted on the tensile peak load, examining the differences between the welded plates with and without an interlayer. The minimum magnitude occurs at p=0.00267 when the gap is 1.0 mm, but the magnitudes are p=0.0756 and 0.0653 for initial gaps equal to 0.5 mm and 1.5 mm, respectively. Not statistically significant, p=0.465 was reached when the gap was equal to zero. The magnitude of the resistance between the welded plates and the current-constriction effect on the generated heat influences nugget growth prior to solidification.

The findings indicated that using iron and TiO_2 interlayers to modify the microstructure and enhance bond strength was more effective than previous research utilizing coated nanoparticles, such as graphene, for welding AISI-1008 material [13][16].

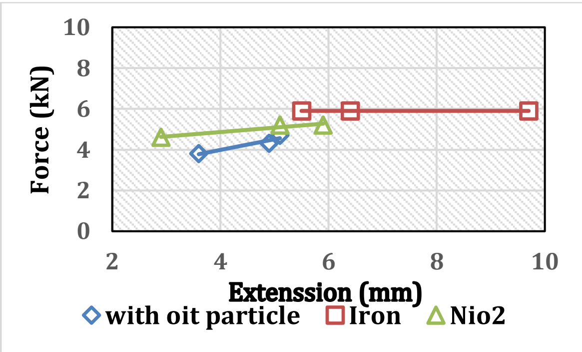

Figure 13. Peak load vs extension for inert particles in spot welding with 1.0 mm gap

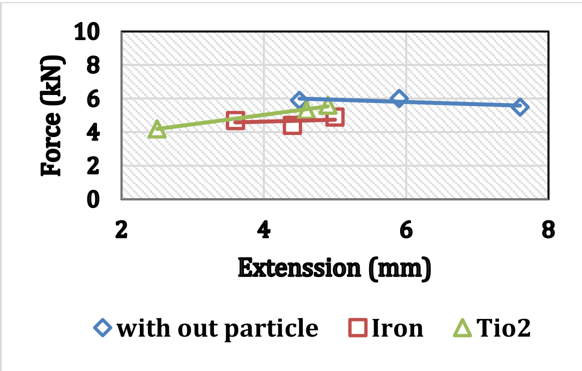

Figure 14. Peak load vs extension for inert particles in spot welding with 1.5 mm gap

The investigation revealed a variation in shear strength resistance by experimental test, along with the differential initial gap magnitude. Moreover, the results clarify the relationship between gap geometry and the additive interlayer process and provide essential experimental data for more precise prediction of failure under shear loads [1][10].

CONCLUSION

In spot resistance welding, the strength of welded plates with an initial gap is affected by incorporating nanoparticles as an intermediate structure. This study examines the interaction among mechanical performance, initial gap magnitude, the characterization of conductive nanoparticles as a filler, and the mechanisms of heat generation and dissipation within the welding zone. The gap- heat – microstructure finding the particular interlayer utilized, offering a credible foundation for predicting the influence of varying gap dimensions on welding efficacy.

1- Gap-Dependent Reinforcement:

In scenarios with the fewest gaps, nanoparticles serve as interlayer fillers. In these situations, nanoparticles play a vital role as mechanical fillers and heat conduits. This improves contact efficiency and elevates Joule heating. Medium gaps enhance the distribution of current density between the welding electrodes, thereby increasing joint strength through thermal concentration.

2- Saturation Thresholds of Gap Dimension:

The heat gradient can explain the microevolution observed during welding. Conductive nanoparticle interlayers facilitate heat concentration and transfer, thereby influencing the cooling rate during solidification, controlling weld zone geometry, and enhancing grain structure. The concentration of grains is directly correlated with interlayer characteristics, thermal transfer rate, initial gap, and weld formation.

3. Theory of Microstructural Evolution:

The thermal gradient produced distinct grain morphologies due to differing heat effects, resulting in an elliptical nugget. The HAZ exhibited transitional microstructural changes between the BM and FZ, while the BM retained elongated ferritic grains resulting from the deep drawing process. There is a relationship between the interlayer and the cooling rate, which influences grain refinement through the creation of an elliptical nugget post-solidification.

4. Relationship Between Hardness and Grain Structure:

The rise in hardness was attributed to grain refinement in the fusion zone, a result of the rapid cooling rate associated with the resistance spot welding method in all welded plates. The hardness of the heat-affected zone and base metal decreases as coarser grains are present.

5. Mechanics of Compaction:

Strength results from the tensile shear test are affected by the addition of nanoparticles, which compact the interlayer by increasing the effective contact area and augmenting the electrical resistance between the welded surfaces.

6. Dynamic Loading Limitation:

The strength of welded plates requires analysis under applied dynamic loads and should factor in impact-resistance fatigue failure.

ETHICAL COMPLIANCE

In our work as researchers, we follow ethical rules at all times, from planning to data collection to analysis to sharing our findings. Respect for people is very important to us in our research.

ACKNOWLEDGMENTS

The authors express their appreciation to the College of Engineering at Kirkuk University for their support during the study. The provided facilities and resources were highly beneficial and pivotal in the effective completion of this research endeavor.

REFERENCES

[1] Su, Y., Song, K., Du, Z., Yu, K., Hu, Z. and Jin, H., "Quantitative study of predicting the effect of the initial gap on mechanical behavior in resistance spot welding based on L-BFGS-B," *Materials*, vol.17, no.19, pp. 4746, 2024, doi: 10.3390/ma17194746.

[2] A. S. Adkine and S. K. Biradar, "A review of the effects of resistance spot welding on metallurgical and mechanical characteristics," *Welding International*, vol. 39, no. 2, pp. 52–65, 2025. doi: 10.1080/09507116.2024.2405623.

[3] T. Das, S. Rawal, S. K. Panda, and J. Paul, "Resistance spot-welding of AISI-1008 steel joints with MWCNT coating interlayer," *Materials and Manufacturing Processes*, vol. 36, no. 4, pp. 448–456, 2021. doi: 10.1080/10426914.2020.1843667.

[4] R. Kumar, J. S. Chohan, R. Goyal, and P. Chauhan, "Impact of process parameters of resistance spot welding on mechanical properties and micro hardness of stainless steel 304 weldments," *International Journal of Structural Integrity*, vol. 12, no. 3, pp. 366–377, 2021, doi: 10.1108/IJSI-03-2020-0031.

[5] M. Shojaee, A. R. H. Midawi, B. Barber, H. Ghassemi-Armaki, M. Worswick, and E. Biro., "Mechanical properties and failure behavior of resistance spot welded third-generation advanced high strength steels," *Journal of Manufacturing Processes*, vol. 65, pp. 364–372, 2021, doi: 10.1016/j.jmapro.2021.03.047.

[6] C. Fan, H. Wang, and D. Ma, "Experimental study of nan electro plating steel spot welding structure under impact tensile-shear loading," *Materials Express*, vol. 11, no. 7, pp. 1207–1213, 2021, doi: 10.1166/mex.2021.2003.

[7] A. Arumugam and A. Pramanik, "A review on the recent trends in forming composite joints using spot welding variants," *Journal of Composites Science*, vol. 8, no. 4, p. 155, 2024. doi: 10.3390/jcs8040155.

[8] K. Yang, Z. Wand, V. Haak, V. Olfert, B. El-Sari, D. Hein, M. Biegler, M. Rethmeier, G. Meschut, "A novel welding schedule for expanding the expulsion-free process window in resistance spot welding of dissimilar joints with ultra-high strength steel," *Journal of Manufacturing Processes,* vol,137, pp. 306-319, 2025, doi: 10.1016/j.jmapro.2025.02.009.

[9] P. Bhavsar, A. Dutta, and S. K. Pal, "Detection of electrode misalignment and its effect on joint quality in resistance spot welding: a low-cost computer vision-based approach," *Measurement Science and Technology*, vol. 35, no. 8, p. 085407, 2024, doi: 10.1088/1361-6501/ad4c86.

[10] Y.J. Xia, Z. Li, W. Wang, T. Yang, G. Pi and Y. Li, "Influence mechanism of initial gap disturbance on the resistance spot welding process," *Automotive Innovation*, vol. 7, no. 2, pp. 360–372, 2024, doi: 10.1007/s42154-023-00264-x.

[11] A. Alzahougi, B. Demir & M. Elitas, "An Optimization Study on Resistance Spot Welding of DP600 Sheet Steel via Experiment and Statistical Analysis," *Engineering, Technology & Applied Science Research*, vol.13, no. 4, pp.11106-11111, 2023, doi: 10.48084/etasr.5804

[12] H. Aliyari, R. Miresmaeili, and M. Azadi, "Fatigue life prediction of spot-welded joints using a novel indentation technique for precise elastoplastic characterization of weld zones," *Journal of Materials Research and Technology*, vol. 35, pp. 2087–2102, 2025., doi: 10.1016/j.jmrt.2025.01.116.

[13] J. Jyoti and B. P. Singh, "A review on 3D graphene–carbon nanotube hybrid polymer nanocomposites," *Journal of Materials science*, vol. 56, pp.17411-17456, 2021, doi: 10.1007/s10853-021-06370-7

[14] M. Oheil, D. Saha, H. Jahed, and A. Gerlich, "Dissimilar resistance spot weld of Ni-coated aluminum to Ni-coated magnesium using cold spray coating technology," *Metals*, vol. 15, no. 9, p. 940, 2025, doi: 10.3390/met15090940

[15] R. Ahmadi and M. Movahedi, "Aluminum–steel resistance spot welding with an aluminum interlayer: simulation and experimental study of weld nugget formation and electrode indentation," *Results in Engineering*, vol. 29, P.109703, 2026, doi: 10.1016/j.rineng.2026.109703

[16] T. Das and J. Paul, "Resistance spot welding of similar and dissimilar metals: the effect of graphene interlayer," *JOM,* The Journal of the Minerals, Metals & Materials Society, vol. 72, pp. 2863–2874, 2020, doi: 10.1007/s11837-020-04159-8.

[17] A. S. Allthari, S. M. Thahab, and A. F. Al-Obbaidi, "Effect of adding TiO_2 nanoparticles on the impact toughness for welding joints of mild steel," *Australian Journal of Mechanical Engineering*, vol. 21, no. 1, pp. 13–26, 2023, doi: 10.1080/14484846.2020.1816734.

[18] B. Lara, R. Giorjao, and A. Ramirez, "Resistance spot welding of printed interlayers to join Al–Fe sheets," *Science and Technology of Welding and Joining*, vol.28, no. 1, pp.18-26, 2023, doi: 10.1080/13621718.2022.2108999.

[19] Y. Yang, Z. Shen, W. Hou, Z. Piao, X. Liu, Y. Guo, G. Huang, X. C. Liu, P. Zhou, H. Li and W. Y. Li, "Role of Zinc Interlayer Reactions on Mechanical Performance of Al/Mg Dissimilar Refill Friction Stir Spot Welds," *JOM*, vol.78, pp. 1291-13.3, 2025, doi: 10.1007/s11837-025-07724-1

[20] L. Li, Y. Tan, and J. Chen, "Microstructure and mechanical properties of resistance spot welded magnesium to aluminum with a nickel-coated steel interlayer," *Journal of Manufacturing Processes*, vol.6, p 381, 2021, doi: 10.1016/j.jmapro.2021.05.012.

[21] T. Das, and J. Paul, "Interlayers in resistance spot-welded lap joints: A critical review," *Metallography, Microstructure, and Analysis*, vol.10, no.1, pp. 3-24, 2021, doi: 10.1007/s13632-021-00714-0

[22] Z. Yao, M. Omiya, N. Ma, P. Geng and Q. Wang, "Local shear fracture properties in heat-affected zone of resistance spot-welded advanced high-strength steel," *Journal of Materials Research and Technology*, vol. 32,

pp. 2200–2213, 2024, doi: 10.1016/j.jmrt.2024.02.035.
[23] *ASTM Standard test methods for tension testing of metallic materials*, E8-/E8M, 2024
[24] C. Rajarajan, P. Sivaraj, T. Sonar, S. Raja and N. Mathiazhagan, "Investigation on microstructural features and tensile shear fracture properties of resistance spot welded advanced high strength dual phase steel sheets," *Journal of the Mechanical Behavior of Materials*, vol. 31, no. 1, pp. 52–63, 2022. doi: 10.1515/jmbm-2022-0006.
[25] A. Arumugam and A. Pramanik, "A review on the recent trends in forming composite joints using spot welding variants," *Journal of Composites Science*, vol. 8, no. 4, p. 155, 2024, doi: 10.3390/jcs8040155.
[26] R. P. Youlia, D. Utami, D. Romahadi, and Y. Xiawei, "A review towards friction stir welding technique: working principle and process parameters," *SINERGi*, vol. 27, no. 3, pp.289-308, 2023. Doi: 10.22441/sinergi.2023.3.001
[27] K. M. Hussein, H. Akbari, R. Noorossana, R. Yadegari and R. Ashiri, "Microhardness and microstructure correlations to the mechanical performance for dissimilar third generation AHSS resistance spot welding," *Journal of Materials Research and Technology*, vol. 30, pp. 7938–7945, 2024, doi: 10.1016/j.jm rt.2024.02.035.
[28] S. Suresh, E. Natarajan, G. Franz, and S. Rajesh, "Differentiation in the SiC filler size effect in the mechanical and tribological properties of friction-spot-welded AA5083-H116 alloy," *Fibers*, vol. 10, no. 12, p. 109, 2022, doi: 10.3390/fib10120109.
[29] P. Manik, A. Firdhaus, B. H. Prasetya, R. Prayoga, "Experimental investigation of PWHT and normalizing effects on SMAW low-carbon steel joint properties," *SINERGI*, vol. 30, no.1, pp.91-102, 2026, doi: 10.22441/sinergi.2026.1.009
[30] O. Sherepenko, A. Mohamadizadeh, A. Zvorykina, M. Worswick, E. Biro and S. Jüttner, "Determination of resistance spot weld failure path in ultra-high-strength press-hardened steel by control of fusion boundary transient softening," *Journal of Materials Science*, vol. 56, no. 25, pp. 14287–14297, 2021, doi: 10.1007/s10853-021-06165-w.
[31 C. T. Rueden, J. Schindelin, M. C. Hiner, B. E. DeZonia, A.E. Walter, E. T. Arena and K. W. Eliceiri, "ImageJ2: Image J for the next generation of scientific image data," *Nature Methods*, vol.18, no.1, p 529, 2020, doi: 10.1038/s41592-017-0045-1.
[32] A. L. Abdullah, S. Radiman, W. S. Chiu, M. A. Abdul Hamid, F. W. Badrudin FW, "Reduced graphene oxide-ZnO hollow microsphere composite for super capacitor applications," *SINERGi*, vol. 29, no. 2, 2025. doi.org/10.22441/sinergi.2025.2.023.
[33] L. I. Alrawi, N. Z. Noriman, M. K. Alomar, A. M. Alakrach, O. S. Dahham, R. Hamzah, B. Betar, T. M. Jassam., "Tensile and morphology properties of PLA/(MM)T-TiO_2 bionano composites," *Defect and Diffusion Forum*, vol. 398, pp. 131–135, 2020, doi: 10.4028/www.scientific.net/DDF.398.131.